Monte Carlo simulation of electron transport in Si/SiO_2 superlattices: Vertical transport enhanced by a parallel field

Marcello Rosini* and Carlo Jacoboni
Istituto Nazionale per la Fisica della Materia, Research Center for nanoStructures and bioSystems at Surfaces (S^3) and Dipartimento di Fisica, Università degli Studi di Modena e Reggio Emilia, via Campi 213/A, 41100 Modena, Italy

Stefano Ossicini
Istituto Nazionale per la Fisica della Materia, Research Center for nanoStructures and bioSystems at Surfaces (S^3) and Dipartimento di Scienze e Metodi dell'Ingegneria, Università degli Studi di Modena e Reggio Emilia, via Allegri 13, 42100 Reggio Emilia, Italy
(Received 22 April 2002; published 30 October 2002)

Considerable effort is presently devoted to develop Si quantum structures for microelectronics and nanoelectronics. In particular, well-defined Si/SiO_2 superlattices and quantum wells are under study. We investigate here the transport properties of a Si/SiO_2 superlattice with a multiband one-particle Monte Carlo simulator. The band structure is obtained with an analytical model and the scattering mechanisms introduced in the simulator are confined optical phonons, both polar and nonpolar. Owing to the very flat shapes of the bands along the growth direction, very low drift velocities are obtained for vertical transport. However, the simulation shows that, for oblique fields, the transport properties along the vertical direction are strongly enhanced by the in-plane component of the electric field, consequently higher vertical drift velocities can be easily obtained.

DOI: 10.1103/PhysRevB.66.155332 PACS number(s): 73.63.Hs, 72.10.Di

I. INTRODUCTION

Silicon is now experiencing a new phase as a functional material. In fact considerable effort is being devoted on the development of efficient silicon light-emitting material.[1–4]

The light-emission processes in silicon are clearly related to quantum confinement effects, thus Si devices based on confined structures, such as quantum layers, quantum wires, or quantum dots, have been the subject of intensive investigations by several research groups.[2–4] Silicon-based heterostructures form one of the most promising classes of such systems because of their easy compatibility with conventional silicon-based integrated circuit technology. In particular, Si/insulator multiple quantum wells or superlattices (SL), where calcium fluoride (CaF_2) or silicon dioxide (SiO_2) were used as insulating material, have been studied from both the experimental and the theoretical points of view, with a particular emphasis on their photoluminescence properties.[5–19] In these systems the thickness of the silicon layers lies in the nanometer range. It is interesting to note that most of the experimental work was originally based on the amorphous silicon films; however, well-defined crystalline Si/SiO_2 systems are now available.[20]

Beside photoluminescence, also electroluminescence has been observed both in Si/CaF_2 and Si/SiO_2 superlattices.[21–26] As the optimization of the electroluminescence is related to the carrier injection efficiency into the Si quantum layers, it is very important to understand the electrical transport properties of these structures. Until now this has been performed by computing current-voltage characteristics both for Si/CaF_2 (Refs. 27 and 28) and Si/SiO_2 (Ref. 29) multiple quantum wells through model calculations, where the electron and hole tunneling between adjacent wells is evaluated within the Wentzel-Kramers-Brillouin approximation[30] or by modeling charge carrier transport across the heterostructures by means of an equivalent circuit.[31] From the numerical results, a number of simple conclusions useful to optimize physical parameters in order to achieve their maximum electroluminescence efficiency has been derived.

Our aim here is to investigate the transport properties of Si/SiO_2 superlattices through a multiband one-particle Monte Carlo simulator in order to study the best response to an applied electric field with respect to the different geometries of the system.

The present work is part of a larger project that will include the study of hole transport and recombination mechanisms, in order to understand electroluminescence properties of silicon-based superlattices.

Section II of this paper is a detailed description of the method used to calculate the band structure of the system. The analytical form of the minibands is obtained by fitting a tight-binding form over the numerical solution obtained within the envelope function formalism. The scattering mechanisms are described in Sec. III, and include in the simulation confined optical phonons, both polar and nonpolar. Section IV focuses on the description of the simulator. Here we show the fundamental steps of the Monte Carlo (MC) simulation, and discuss how scattering events are included in the code.

In Sec. V, we present our results concerning simulations with vertically applied field and oblique field, where we can see the effect of the parallel component of the electric field on vertical transport. In particular, we show that in this way we can significantly improve vertical transport properties.

II. BAND STRUCTURE

The material under investigation is a Si/SiO_2 SL, where the Si layers are grown along the (100) direction z.

As Hamiltonian for an electron in our SL, we assume the following:

$$H_{SL} = H_{cr} + W_{SL} + H_{e-p}, \tag{1}$$

where H_{cr} is the Hamiltonian due to the crystalline potential, W_{SL} is the SL potential, and $H_{e\text{-}p}$ is the electron-phonon interaction Hamiltonian. The interaction with phonons is treated within the time-dependent perturbation theory and will be developed in the following section.

Now, the Schrödinger equation to be solved is

$$[H_{cr}(\mathbf{r}) + W_{SL}(\mathbf{r})]|\Psi\rangle = E|\Psi\rangle. \tag{2}$$

If we consider that the electrons moves near a band minimum $\mathbf{k}_0$, we can apply the *envelope function approximation*[32] to solve the problem, obtaining a new equation that describes the eigenvalue problem for the envelope function:

$$[E_n(-i\boldsymbol{\nabla}) + W_{SL}(\mathbf{r})]\mathcal{F}_n(\mathbf{r}) = E\mathcal{F}_n(\mathbf{r}), \tag{3}$$

where $\mathcal{F}$ is the envelope function and $E_n(-i\boldsymbol{\nabla})$ is the energy operator for the electron in the material. The expression for this last operator, when considering a little interval near a minimum $\mathbf{k}_0$, can be easily substituted by the parabolic band approximation,[33]

$$E_n(-i\boldsymbol{\nabla}) \simeq E_n(\mathbf{k}_0) + (-i\boldsymbol{\nabla}_i - k_{0,i})\left(\frac{\hbar^2}{2m^*}\right)_{i,j}(-i\boldsymbol{\nabla}_j - k_{0,j}). \tag{4}$$

The effective mass tensor $(1/m^*)_{i,j}$ describes the band curving around the point $\mathbf{k}_0$. Equation (3) is separable along the high symmetry of $1/m^*$ directions and allows us to deal with one-dimensional problems.

First, let us look for the solution along the SL growth direction z. The effective mass is now a function of the material layer and, in general, it may be considered as a function of the z position; the new problem to be solved is

$$\left(-\frac{\hbar^2}{2}\boldsymbol{\nabla}\frac{1}{m(z)}\boldsymbol{\nabla} + W_{SL}(z)\right)\mathcal{F}(z) = E_z\mathcal{F}(z), \tag{5}$$

where the term $\boldsymbol{\nabla}[1/m(z)]\boldsymbol{\nabla}$ ensures current continuity at the interfaces,[34] and the potential W_{SL} is the Krönig-Penney potential:

$$W_{SL}(z) = \begin{cases} 0, & -b \leqslant z - nL \leqslant 0 \\ W_0, & 0 \leqslant z - nL \leqslant a, \end{cases} \tag{6}$$

where W_0 is the conduction-band offset (CBO). With current conservation[34] and periodic-boundary conditions, we get the solution along the z direction, i.e., the minibands $E(k_z)$.

Concerning the x and y problems, we notice that Eq. (5) along these directions represents a free-electron problem, so we get a parabolic dispersion. Therefore, the resulting three-dimensional (3D) miniband is

$$E(\mathbf{k}) = E(k_z) + \frac{\hbar^2}{2m_x}(k_x - k_{x,0})^2 + \frac{\hbar^2}{2m_y}(k_y - k_{y,0})^2, \tag{7}$$

where $E(k_z)$ is the nonanalytical solution of the Krönig-Penney[35] potential. This expression can be approximated by a tight-binding[36] analytical dispersion $E(k_z) \simeq \tilde{\epsilon} - \tilde{t}\cos(k_z d)$, where $\tilde{\epsilon}$ and $\tilde{t}$ are, respectively, the middle energy and the half width of the miniband, and are used as parameters fitted to the Krönig-Penney solution. In the case of silicon we must consider that the six band minima are off-Γ. The jth miniband arising from the αth minimum, centered in $\mathbf{k}_0^\alpha$, has the analytical form

$$E_j^\alpha(\mathbf{k}) = \frac{\hbar^2}{2m_x^\alpha}(k_x - k_{0,x}^\alpha)^2 + \frac{\hbar^2}{2m_y^\alpha}(k_y - k_{0,y}^\alpha)^2 + [\tilde{\epsilon}_j^\alpha - \tilde{t}_j^\alpha\cos(k_z d)]. \tag{8}$$

It is evident that, along the z direction, all the equivalent valleys of silicon are refolded in $k_z = 0$, while the positions $k_{0,x}^\alpha$ and $k_{0,y}^\alpha$ do not change. As a consequence, if the SL is grown along the Si (001) direction, the two valleys along k_z are refolded into the same miniband with double multiplicity. Although the six silicon valleys have the same energy, in the SL they have different energies owing to the different effective masses along the z direction. The minibands for a Si/SiO_2 SL (with 24-Å Si and 7.68-Å SiO_2) are represented in Fig. 1. In this figure only the dispersion along k_z is represented so the continuous and the dotted lines are the dispersions of the bands centered at Γ, the dashed line is the dispersion for the fourfold minibands off-Γ. These minibands are very flat, in particular, the lowest one that is about 1 meV wide. This is the cause of very low vertical mobility in such systems.

III. SCATTERING MECHANISMS

The system under examination is supposed to be a perfectly grown SL with smooth interfaces, so we can assume that there is no interface scattering. We also consider a SL grown with a content of impurity so low that at room temperature, impurity scattering is negligible if compared to the phonon scattering. As regards scattering by phonons, in our simulations we include only optical-phonon scattering because at room temperature this is the strongest mechanism.

Optical phonons in layered systems are generally confined,[37,38] it means that silicon layers will show optical frequencies typical of a bulk silicon and oxide layers will behave as a bulk oxide. For this reason, during the simulation, we account for the real-space position of the electron; when it moves within the Si layers, it can interact with Si phonons and, in the oxide layers, with oxide optical phonons.[53]

Since Si is a nonpolar material, the electrons in the Si layer can interact with the lattice only via deformation potential; SiO_2 is a polar material and the electrons interact both with polar and deformation potential mechanisms.[39] Actually, in the silicon dioxide two polar phonons modes, and

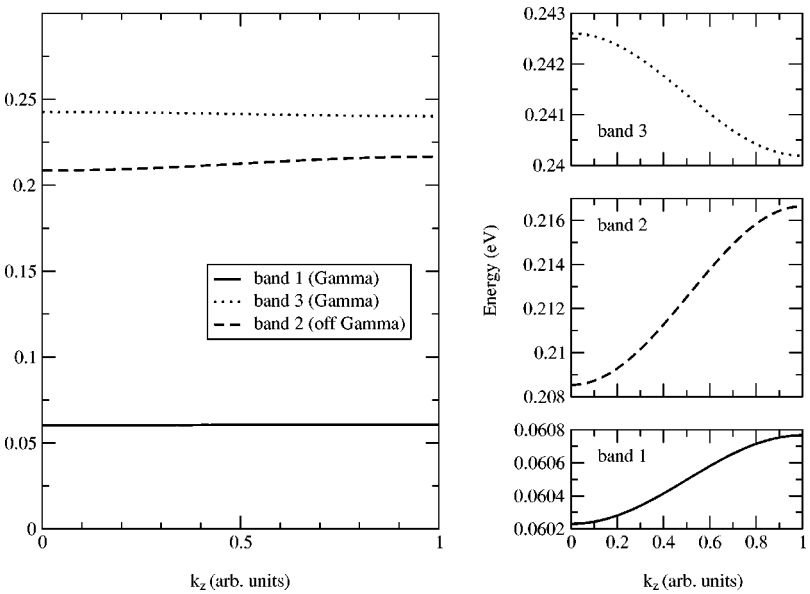

FIG. 1. k_z dispersion of the minibands. The dashed line represents the z dispersion of the (100) and (010) valleys. Note the different scales in the three figures on the right showing zooms on the minibands.

one nonpolar, are present (the specific constants are given in Table I).

The optical-phonon differential scattering rate is obtained by using the Fermi golden rule,

$$P(n\mathbf{k};n'\mathbf{k}')=\frac{2\pi}{\hbar}M(n\mathbf{k};n'\mathbf{k}')\delta[E_n(\mathbf{k})-E_{n'}(\mathbf{k}')\pm\hbar\omega_{op}], \tag{9}$$

where $M(n\mathbf{k};n'\mathbf{k}')=|\langle n'\mathbf{k}'|H_{e\text{-}p}|n\mathbf{k}\rangle|^2$. (Here and in the following, n will indicate a specific miniband that is the pair of labels α and j.) In particular, if we substitute the miniband dispersion (8) into the δ function and integrate over $\mathbf{k}'$, we obtain the total scattering rate for an electron that is scattered by a phonon of energy $\hbar\omega$ from the n miniband and pseudomomentum $\mathbf{k}$ into any $\mathbf{k}'$ in the n' miniband.

The matrix element for deformation potential optical phonons is[40]

$$|M_{n,n'}(\mathbf{k},\mathbf{k}')|^2=\frac{\hbar(D_tK)^2}{2\rho V\omega_{op}}\begin{bmatrix}N_{op}\\N_{op}+1\end{bmatrix}, \tag{10}$$

and for polar optical phonon is

TABLE I. Values used in the simulations for the physical quantities.

Physical quantity	Value/Ref.
Longitudinal effective mass in Si	$m^*=0.97$ (Ref. 41)
Transverse effective mass in Si	$m^*=0.19$ (Ref. 41)
Effective mass in SiO_2	$m^*=0.3$, (Refs. 42,43)
Conduction-band offset	CBO$=3.1$ eV (Ref. 44)
Lattice temperature	$T=300$ K
Si optical-phonon energy	$E=60$ meV (Ref. 45)
Si optical coupling constant	$D_tK=8\times10^8$ eV/cm (Ref. 45)
Oxide nonpolar phonon energy	$E=132$ meV (Ref. 39)
Oxide optical coupling constant	$D_tK=2\times10^9$ eV/cm (Ref. 39)
Oxide first polar phonon energy	$E=63$ meV (Ref. 39)
First polar optical constant	$\frac{1}{\epsilon_+}-\frac{1}{\epsilon_-}=0.063$ (Ref. 39)
Oxide second polar phonon energy	$E=153$ meV (Ref. 39)
Second polar optical constant	$\frac{1}{\epsilon_+}-\frac{1}{\epsilon_-}=0.143$ (Ref. 39)
Oxide mean polar phonon energy	$E=108$ meV
Mean polar optical constant	$\frac{1}{\epsilon_+}-\frac{1}{\epsilon_-}=0.2$
Oxide screening wave vector	10^9 cm^{-1}

[a]Arbitrarily chosen in order to avoid divergences. This value implies a carrier concentration near 10^{16} cm^{-3}, typical of doped silicon. We have performed simulations with the correct screening length for undoped silicon and the results are almost the same, but the simulation time is one order of magnitude larger.

$$|M_{nn'}(\mathbf{k},\mathbf{k}')|^2 = \frac{e^2 E_{op}}{2V(|\mathbf{k}-\mathbf{k}'|^2+|\mathbf{k}_D|^2)}\left(\frac{1}{\epsilon_+}-\frac{1}{\epsilon_-}\right)\begin{bmatrix} N_{op} \\ N_{op}+1 \end{bmatrix}, \tag{11}$$

where $D_t K$ is the deformation potential coupling constant, N_{op} is the phonon population, $\mathbf{k}_D = 1/l_D$ is the screening wave vector for the electrons, and ϵ_- and ϵ_+ are the low- and high-frequency dielectric constants. In this way, both interband and intraband scattering probabilities have been introduced.

IV. THE MONTE CARLO SIMULATOR

An electron subject to the electric field is accelerated along the field direction, but it remains in the same miniband. When a scattering occurs, the ballistic flight is interrupted and the electron is scattered away into a $\mathbf{k}'$ point in the same or in another miniband; then the particle is again accelerated by the electric field.

We performed the simulation of transport using a semiclassical one-particle MC.[45] According to this general scheme, we randomly generate the free flight duration $t_r = (1/\Gamma_0)\ln(r)$ (Γ_0 is the total scattering rate including the self-scattering mechanism). Now we choose randomly the scattering mechanism and the state after the collision according to the differential scattering rate $P_{n'}(\mathbf{k},\mathbf{k}')$ of the selected process.

After integration of Eq. (9), the nonpolar scattering probability results in

$$P_{n'}(E) = \frac{(D_t k)^2}{2\rho\omega_{op}\hbar^2 d}\sqrt{m_x^{n'} m_y^{n'}}\begin{bmatrix} N_{op} \\ N_{op}+1 \end{bmatrix} \times \begin{cases} 0 \\ \frac{1}{\pi}\arccos\left(\frac{E_{n'}-E\mp\hbar\omega}{|\tilde{t}_{n'}|}\right) \\ 1 \end{cases}. \tag{12}$$

In the integration of the total scattering rate, we have to sum over all the minibands n', counted with their multiplicity m: $P(E) = \Sigma_{n'} m_{n'} P_{n'}(E)$.

The polar optical interaction in Eq. (11) gives rise to an anisotropic scattering rate. In order to simplify the calculation, we maximize the matrix element by imposing $\mathbf{k}-\mathbf{k}' = 0$ and now the integration is the same than before with maximized probability:

$$\overline{P}(E) = \frac{\pi e^2 \omega_{op}}{2d\hbar^2 k_D^2}\left(\frac{1}{\epsilon_+}-\frac{1}{\epsilon_-}\right)\sqrt{m_x^{n'} m_y^{n'}}\begin{bmatrix} N_{op} \\ N_{op}+1 \end{bmatrix} \times \begin{cases} 0 \\ \frac{1}{\pi}\arccos\left(\frac{E_{n'}-E\mp\hbar\omega}{|\tilde{t}_{\beta}|}\right) \\ 1 \end{cases}. \tag{13}$$

To get the exact result, once the state after the scattering $\mathbf{k}'$ is generated, we apply the rejection technique in order to decide whether the scattering process, or a fictitious self-scattering, has occurred. The optical-phonon dispersions are approximated, as usual, with constants, and the two polar phonons in oxide are introduced in the simulation as only one mode of mean energy and the coupling constant equal to the sum of the two constants (see Table I). The final scattering rate reveals a steplike behavior typical of the density of states of our system.

The estimators for the physical quantities are collected at the end of each free flight, just before the choice of the scattering mechanism, even if the flight ends with a self-scattering. In the simulation we are interested in the drift velocity, the mean energy, and the electron distribution functions in energy and in momentum space. The two distribution functions are obtained by setting up meshes on energy and momenta and counting how many times the electron visits each interval of these meshes. The mean energy is $\overline{\epsilon} = (1/N)\Sigma_{i=1}^{N}\epsilon_i$, where N is the number of free flights in the simulation and ϵ_i is the energy at the end of the flight. The drift velocity is obtained[45] from the same estimator by substitution of energy with the group velocity $\mathbf{v}_g = (1/\hbar)\nabla_{\mathbf{k}}\epsilon(\mathbf{k})$. The simulation time is long enough to ensure the physical quantities to have small statistical errors, typically the error associated to our results is of the order of 0.1–1 %.

V. RESULTS AND DISCUSSION

Two kinds of simulations have been performed: (a) with the field applied along the growth direction z, and (b) with an oblique field. In the latter case, a constant field is applied along the z direction and a component of the field in the parallel x direction is varied. In both cases, vertical transport is studied. Simulations are performed at lattice temperature $T = 300$ K. The model has been tested for $GaAs/Al_xGa_{1-x}As$ SL's and our results are in good agreement with experiments[46] and theoretical predictions.[47] The two different geometries, with different layer thicknesses, have been considered for Si/SiO_2 superlattice.

A. (25/5)-Å SL with vertical fields

The first system studied is a SL arbitrarily made up of 25 Å of silicon and 5 Å of silicon dioxide with an applied vertical electric field; the results are shown in Figs. 2 and 3. As it regards drift velocity (Fig. 2, lower part), we see that increasing the electric field, the velocity first increases up to a maximum and then a further increase of the applied field causes a decrease in the drift velocity. This is the negative differential conductivity regime, predicted by Esaki and Tsu,[48] and it can be explained using the electronic distribution function in k_z direction (Fig. 3 lower part): at low electric field the distribution is located near the center of the minizone, but slightly shifted towards right, so the drift velocity is low. At higher field the peak of the distribution is more shifted where the group velocity is higher; then, for highest field the maximum shifts, but the distribution flattens

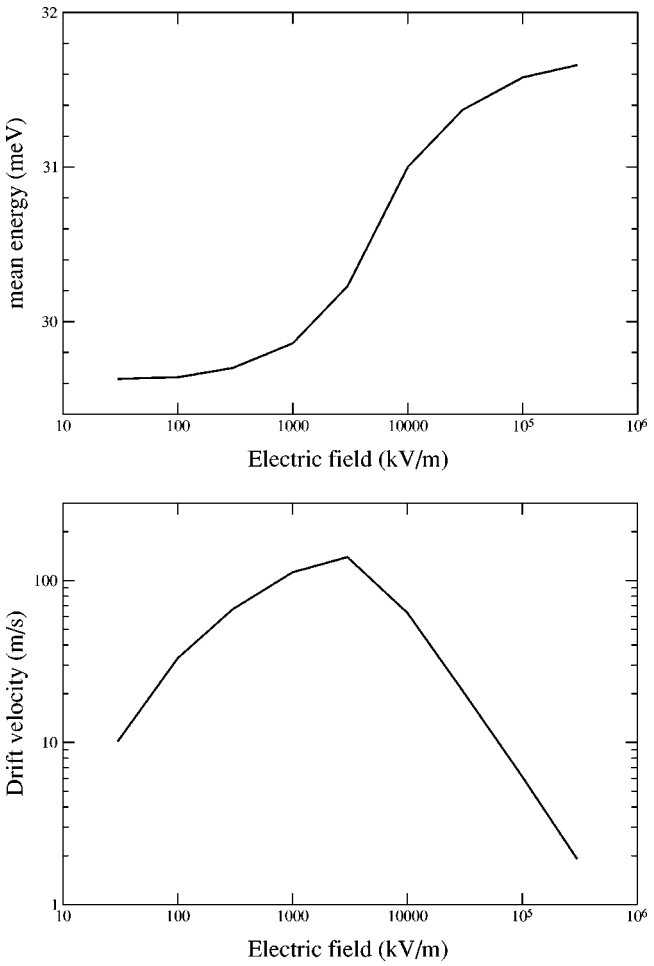

FIG. 2. Mean energy (measured from the minimum of the lowest band) and drift velocity for a (25/5)-Å Si/SiO_2 SL.

and the drift velocity comes from the contribution of all the *k*-space points. Another important result is that drift velocity is very low, owing to the very flat shape of the miniband.

The mean energy assumes a value near 28 meV in the region of low fields, then it increases about 1.5 meV (Fig. 2);

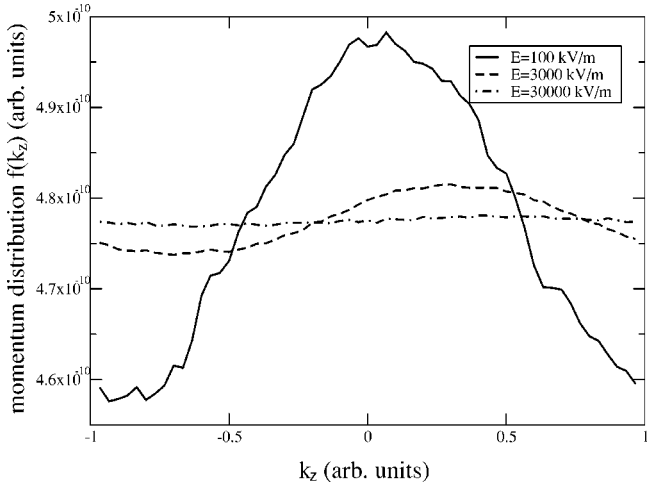

FIG. 3. Momentum distribution functions for the (25/5)-Å Si/SiO_2 SL, for several values of the applied field.

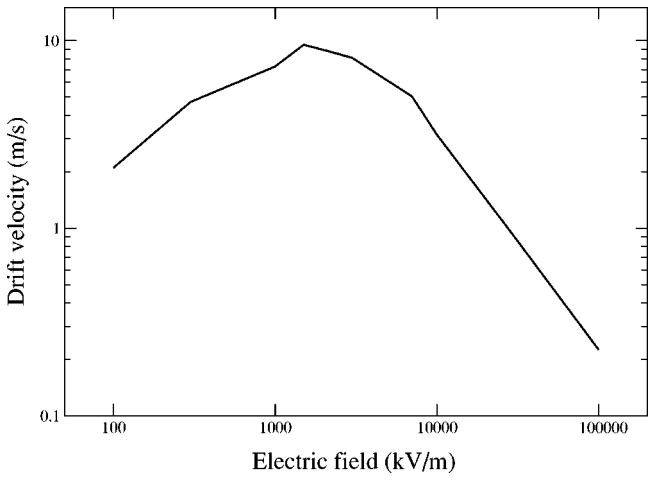

FIG. 4. Drift velocity for a (24/7.68)-Å Si/SiO_2 SL.

this increase cannot be observed in the energy distribution function because it is very small.

Figure 2, upper part, shows the mean electron energy as a function of the electric field. Since the system under investigation has parabolic energy dispersion along two directions and a different, very flat, dispersion along *z* direction, it is of interest to analyze the mean kinetic energy at equilibrium. This analysis is presented in the Appendix. The energy shown in Fig. 2 is the total energy (including miniband bottoms) measured from the bottom of the lowest miniband, so that the equilibrium value (around 29 meV) is slightly above the two-dimensional case, consistently with the fact that upper minibands are partially occupied. The increase observed in mean energy can be interpreted noting that it is comparable to the miniband width and that, as described above, at high fields, electrons populates uniformly the whole miniband.

B. (24/7.68)-Å SL with vertical fields

The second system analyzed in this work has almost the same thickness of silicon and a larger thickness of oxide, so we can study the dependence of transport properties upon the dimensions of the system. Moreover, the dimensions are now directly correlated to the material unit cells; the two layer thicknesses correspond, respectively, to exactly 4.5 times the dimension of the Si unit cell and one SiO_2 unit cell. The results are reported in Figs. 4–6. With vertical applied field the behavior for the drift velocity (Fig. 4) is similar, but the intensity is one order of magnitude lower. This low transport regime is caused by the larger barriers (7.68 Å versus 5 Å) that implies more flat minibands, or equivalently, reduction of the tunneling rate.

We have reported the drift velocity in each miniband (Fig. 5) and the population of electrons in each miniband (Fig. 6). It can be seen that the higher minibands, having higher velocities, are less populated so their contribution to the overall drift velocity is very low at low fields, when the field is increased, the second miniband gives the most important contribution to the drift velocity.

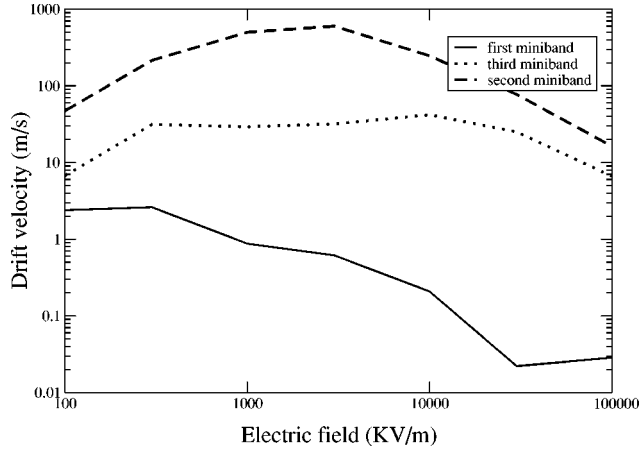

FIG. 5. Drift velocity, for each miniband, in a (24/7.68)-Å Si/SiO_2 SL.

The momentum distribution function has very similar behavior to that found in case described in the preceding section.

C. (24/7.68)-Å SL with oblique fields

We have seen in the previous sections that the vertical transport properties are in general very weak when only vertical field is applied. The idea we propose in this section is that by applying a parallel field, electrons can be heated up and populate higher (and wider) minibands. This gives rise to a higher mobility. In other words, by increasing the electron energy, tunneling is favored.

Concerning diagonal simulations, we consider the latter SL, with a constant field along the z direction $E_z = 2000$ KV/m, near the peak of the velocity curve. We also apply a variable field along the x direction, so that we can study the vertical transport versus parallel electric field. The system is anisotropic and the electron mobility is much higher along the in-plane direction, about three or four orders of magnitude higher than along the vertical direction; the resulting drift velocity is not parallel to the electric field. A typical result with $E_z = 3000$ KV/m and $E_x = 200$ KV/m is a drift velocity of $v_{d,z} = 6.5$ m/s and $v_{d,x} = 60\,000$ m/s. From what has been said above, it is very interesting to study how the z component of the velocity is influenced by the parallel electric field; these results are showed in Figs. 7–12.

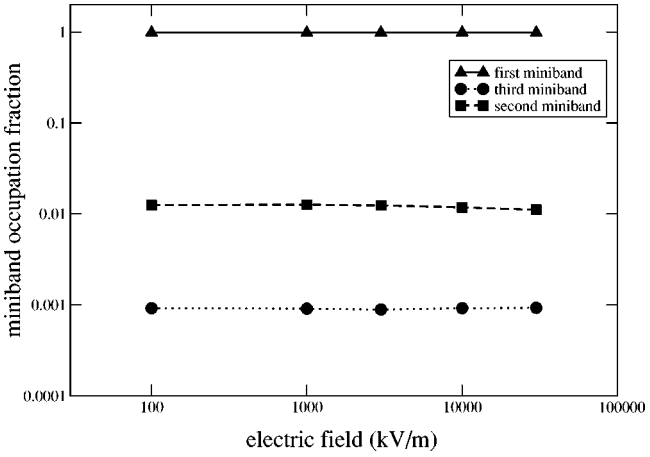

FIG. 6. Population in the minibands for the (24/7.68)-Å Si/SiO_2 SL.

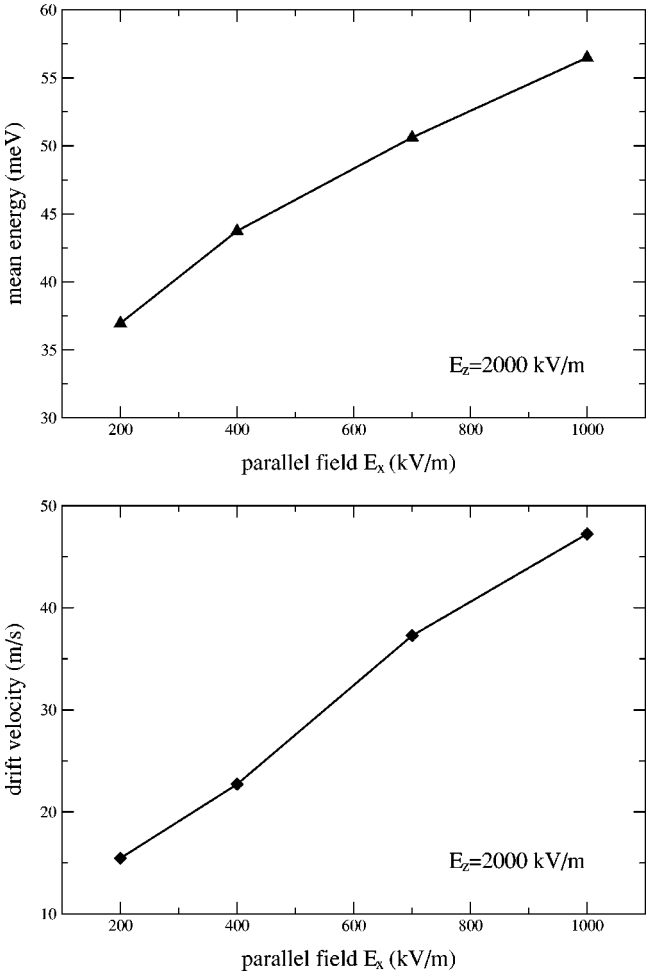

FIG. 7. Mean energy and drift velocity as functions of the parallel field with constant field along z direction, for a (24/7.68)-Å Si/SiO_2 SL.

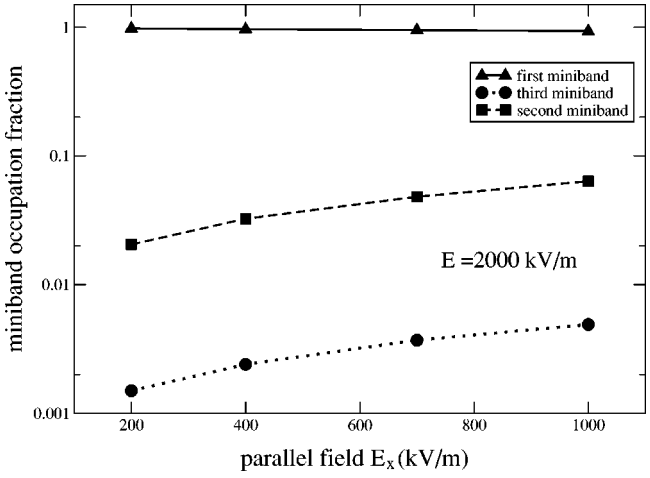

FIG. 8. Population fraction for a (24/7.68)-Å Si/SiO_2 SL.

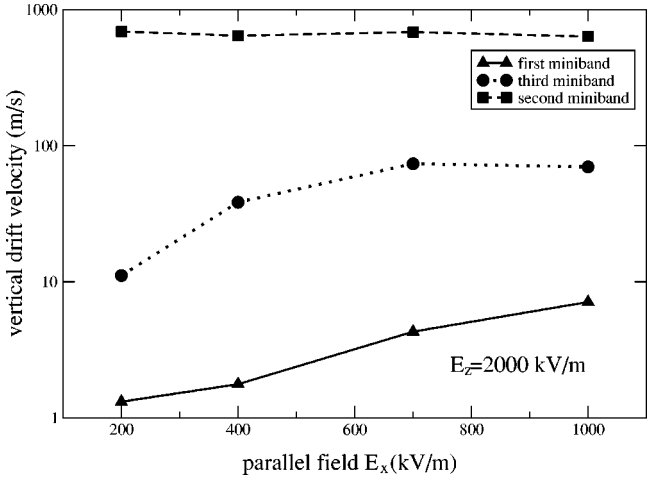

FIG. 9. Drift velocity for each miniband in a (24/7.68)-Å Si/SiO_2 SL.

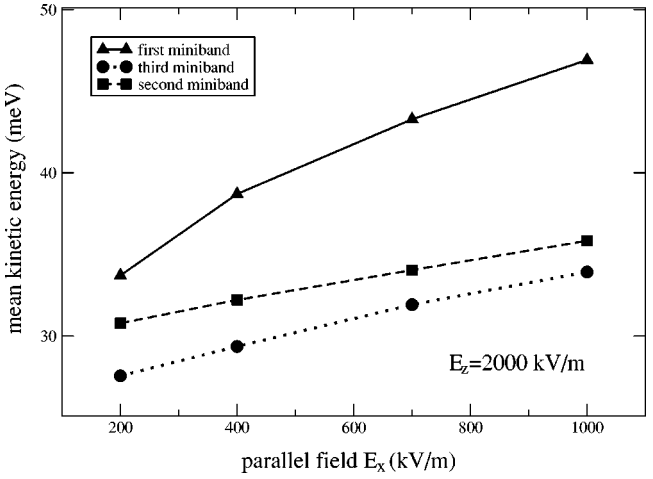

FIG. 11. Mean energy, above the bottom of each miniband, in a (24/7.7)-Å Si/SiO_2 SL.

As it regards drift velocity (Fig. 7 lower part), we see that, when a lateral field is applied, electrons move twice or three times faster than with only vertical field. This phenomenon is clearly interpreted by observing the miniband populations versus parallel electric field (Fig. 8), the drift velocity separated for each miniband (Fig. 9) and the momentum distribution functions (Fig. 10) as function of *E*.

Electrons move faster, by increasing the field, for two reasons: the first one is that by increasing the parallel field, the fractions of electron populations in higher minibands increase, thus ''faster'' minibands give a more important contribution to transport; moreover, it can be seen that the value of drift velocity provided by each miniband increases by itself (Fig. 9) owing to the change in the momentum distribution for each miniband (Fig. 10). The parallel electric field unbalances the momentum distribution favoring the regions with positive velocity.

This interpretation is confirmed by the heating of electrons reported in Figs. 7, 11, and 12 showing, respectively, the total kinetic energy, the kinetic energy for each miniband, and the energy distribution functions; electrons are heated up in each miniband, and the wider minibands contribute more when the parallel field increases. The heating occurs along the parallel direction and redistribute itself in the other directions.

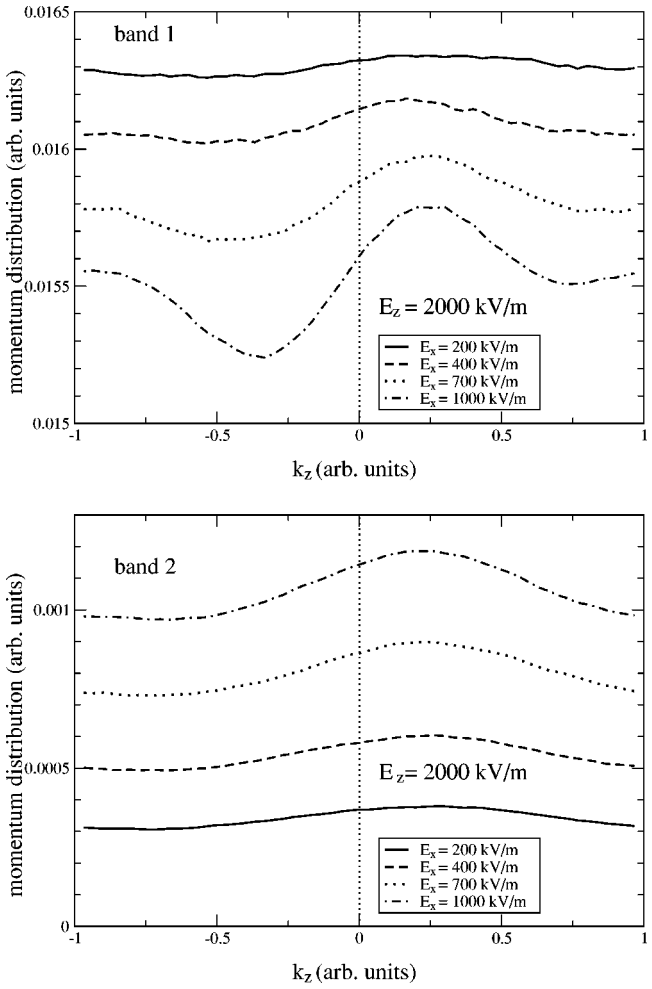

FIG. 10. Momentum distribution function, in the miniband 1 and 2, for several values of parallel electric field E_x.

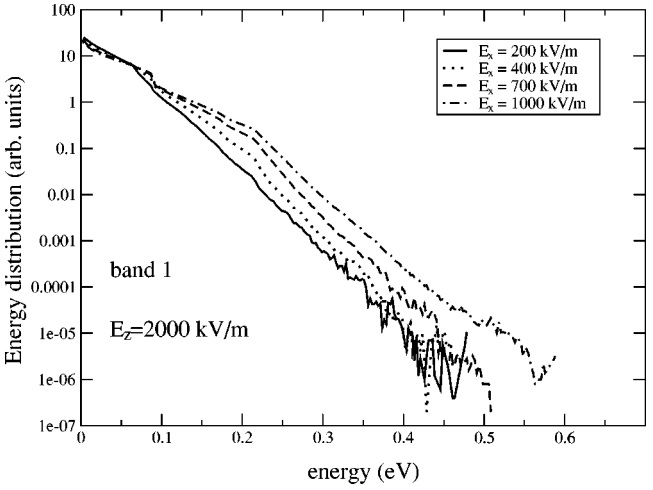

FIG. 12. Energy distribution function, in the first miniband, for several values of parallel electric field E_x.

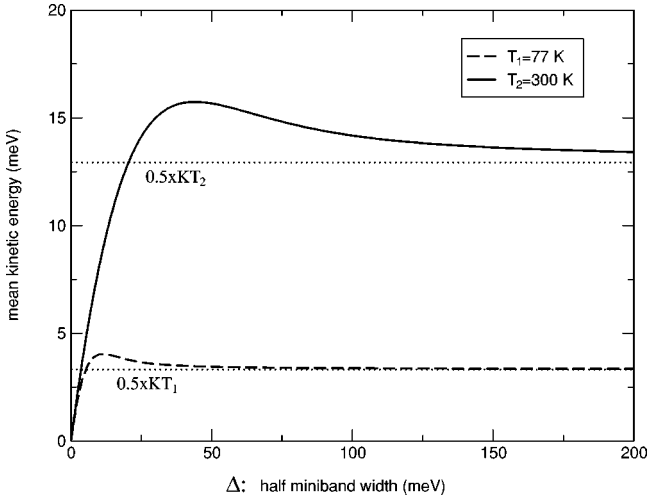

FIG. 13. Mean kinetic energy in a SL miniband vs Δ (half of the miniband width).

In Fig. 12, the distribution functions, especially at high parallel field, for the first miniband show different slopes separated by kinks. This behavior is strongly dependent on the phonon-scattering rate. Electrons with energy below the first kink have little possibility to dissipate because they cannot emit optical phonons; above this energy, their thermalization is more efficient through phonon emission. The second kink arises from the same mechanism with the final state in the second miniband.

VI. CONCLUSIONS

In this work we have investigated the electrical response of Si/SiO_2 superlattice to applied electric fields. Two different geometries have been studied, in which the silicon and oxide layers have different thicknesses. Coherently with the very flat shape of the miniband, we found low drift velocity. Moreover, the mean velocity of electron in strongly dependent upon the oxide layer thickness: it decreases significantly when the oxide layers are thicker. The curve of the drift velocity is well explained by the Esaki-Tsu model.

Now we discuss the validity of the model used in this paper. The semiclassical miniband transport description is useful when the miniband width is greater than the voltage drop over a SL period, i.e., $eEd<2\tilde{t}$; beyond this limit, a quantum description is required.[49] The first miniband (that is less than 1 meV wide) satisfies this condition for fields lower than 200 KV/m. But from the Figs. 4 and 5, it is possible to see that above this value the transport properties are dominated by the second miniband. This miniband is about 9 meV wide and satisfies the former condition when E_z <3000 KV/m. Since in the diagonal simulations a vertical field $E_z=2000$ KV/m is used, the semiclassical model should be applicable. For higher electric fields, the results of a rigorous quantum theory could be somewhat different, but we are confident that the major physical result presented here would be confirmed.

We have shown that it is possible to improve transport, by applying an extra component of the electric field, parallel to the layer interfaces. In this way, a better vertical drift velocity has been obtained through an increase of electron energy. Our discussion has shown that this is caused by the in-plane heating of the carriers in such a way that can populate higher minibands. From the experimental point of view, electric field is a way for this purpose, probably similar results could be obtained using alternated electric fields.

ACKNOWLEDGMENT

This work has been partially supported by the INFM-PRA RAMSES.

APPENDIX: MEAN KINETIC ENERGY IN SL MINIBANDS

The SL under investigation is a quasi-2D system: the electron dispersion is parabolic in the *x*-*y* plane and a nearly flat cosine shape in the *z* direction. So we can expect a mean value for kinetic energy *K*, between the two dimensional k_BT and the three dimensional $\frac{3}{2}k_BT$. In this section, we perform this calculation. The starting point is the standard statistical definition[50]

$$\overline{K}=-\frac{\partial}{\partial\beta}\ln\int_{-\infty}^{+\infty}e^{-\beta\epsilon(\mathbf{p})}d\mathbf{p}. \tag{A1}$$

The electron kinetic energy is measured starting from the minimum of the miniband. Equation (8) can be rewritten as $\epsilon(\mathbf{p})=\epsilon_x+\epsilon_y+\Delta[1-\cos(p_z/\hbar)d]$ [where $\Delta=\tilde{t}$ in Eq. 8], and the above definition becomes

$$\overline{K}=-\sum_{i=1}^{3}\frac{\partial}{\partial\beta}\ln\int_{-\infty}^{+\infty}e^{-\beta\epsilon_i(p_i)}dp_i=\sum_{i=1}^{3}K_i=\frac{1}{\beta}+K_3. \tag{A2}$$

The mean kinetic energy is $K_x=K_y=1/\beta$ for the parabolic degrees of freedom, while for the *z* direction it is

$$\overline{K_z}=\Delta-\frac{\partial}{\partial\beta}\ln I(\beta,\Delta), \tag{A3}$$

where

$$I(\beta,\Delta)=2\frac{\hbar}{d}\int_0^{\pi}e^{\beta\Delta\cos\xi}d\xi. \tag{A4}$$

If we perform the substitution $c=-\cos(\xi)$,

$$I(\beta,\Delta)=2\frac{\hbar}{d}\int_{-1}^{1}(1-c^2)^{-1/2}e^{\beta\Delta c}dc=2\frac{\hbar}{d}\sqrt{\pi}\Gamma\left(\frac{1}{2}\right)\mathcal{I}_0(\beta\Delta), \tag{A5}$$

here Γ is the factorial function and $\mathcal{I}_0(\beta\Delta)$ is the Bessel function. Substituting the last result in Eq. (A3), and remem-

bering $1/\beta = k_B T$, we have the final form

$$\overline{K}_z(T,\Delta) = \Delta - \left[\frac{\partial}{\partial\beta}\ln \mathcal{I}_0(\beta\Delta)\right]_{\beta=1/k_B T}. \qquad \text{(A6)}$$

The result can be plotted numerically (Fig. 13): the graph shows that for low Δ the 1D kinetic energy is between 0 and $k_B T$. This value increase with Δ and becomes greater than $k_B T$; this is due to the particular form of the miniband.

*Electronic mail: mrosini@unimo.it

[1] P. Ball, Nature (London) **409**, 974 (2001).

[2] D.J. Lockwood, *Light Emission in Silicon: From Physics to Devices* (Academic Press, London, 1998).

[3] O. Bisi, S.U. Campisano, L. Pavesi, and F. Priolo, *Silicon Based Microphotonics: From Basics to Applications* (IOS Press, Amsterdam, 1999).

[4] O. Bisi, S. Ossicini, and L. Pavesi, Surf. Sci. Rep. **38**, 5 (2000).

[5] R. Tsu, Nature (London) **364**, 19 (1993).

[6] S. Ossicini, A. Fasolino, and F. Bernardini, Phys. Rev. Lett. **72**, 1044 (1994).

[7] F.A. d'Avitaya, L. Vervoort, F. Bassani, S. Ossicini, A. Fasolino, and F. Bernardini, Europhys. Lett. **31**, 25 (1995).

[8] L. Vervoort, F. Bassani, I. Mihalchescu, J.C. Vial, and F.A. d'Avitaya, Phys. Status Solidi B **190**, 123 (1995).

[9] F. Bassani, L. Vervoort, I. Mihalchescu, J.C. Vial, and F.A. d'Avitaya, J. Appl. Phys. **79**, 4066 (1996).

[10] D.J. Lockwood, Z.H. Lu, and J.M. Baribeau, Phys. Rev. Lett. **76**, 539 (1996).

[11] S.V. Novikov, J. Sinkkonen, O. Kilpela, and S.V. Gastev, J. Vac. Sci. Technol. B **15**, 1471 (1997).

[12] E. Degoli and S. Ossicini, Phys. Rev. B **57**, 14 776 (1998).

[13] H. Kageshima and K. Shiraishi, Phys. Rev. Lett. **81**, 5936 (1998).

[14] N. Tit and M.W.C.D. Wardana, Solid State Commun. **106**, 191 (1998).

[15] A.G. Nassiopoulou, V. Ioannou-Sougleridis, P. Photopoulos, A. Travlos, V. Tsakiri, and D. Papadimitriou, Phys. Status Solidi B **165**, 79 (1998).

[16] L. Tsybeskov, K.D. Hirschmann, S.P. Duttagupta, M. Zacharias, P.M. Fauchet, J.P.M. Caffrey, and D.J. Lockwood, Appl. Phys. Lett. **72**, 43 (1998).

[17] G. Pucker, M. Cazzanelli, P. Belletti, K. Gatterer, C. Spinella, and L. Pavesi, J. Appl. Phys. **88**, 6044 (2000).

[18] V. Mulloni, R. Chierchia, C. Mazzoleni, G. Pucker, and L. Pavesi, Philos. Mag. A **80**, 705 (2000).

[19] E. Degoli and S. Ossicini, Surf. Sci. **479**, 32 (2000).

[20] Z.H. Lu and D. Grozea, Appl. Phys. Lett. **80**, 255 (2002).

[21] A.G. Nassiopoulou, V. Tsakiri, V. Ioannou-Sougleridis, P. Photopoulos, S. Menard, F. Bassani, and F.A. d'Avitaya, J. Lumin. **80**, 81 (1998).

[22] S. Menard, M. Liniger, F. Bassani, F.A. d'Avitaya, A.N. Kholod, and V.E. Borisenko, Mater. Sci. Eng., B **B69-B70**, 464 (2000).

[23] P. Photopoulos, A.G. Nassiopoulou, D.N. Kouvastsos, and A. Travlos, Appl. Phys. Lett. **76**, 3588 (2000).

[24] P. Photopoulos, A.G. Nassiopoulou, D.N. Kouvastsos, and A. Travlos, Mater. Sci. Eng., B **B69-B70**, 345 (2000).

[25] C.L. Heng, Y.K. Sun, T. Wang, Y. Chen, Y.P. Qiao, B.R. Zang, Z.C. Ma, W.H. Zong, and G.G. Qin, Appl. Phys. Lett. **77**, 1416 (2000).

[26] G. Pucker, P. Bellutti, M. Cazzanelli, Z. Gaburro, and L. Pavesi, Opt. Mater. **17**, 27 (2000).

[27] A.N. Kholod, A.L. Danilyuk, V.E. Borisenko, F. Bassani, S. Menard, and F.A. d'Avitaya, J. Appl. Phys. **85**, 7219 (1999).

[28] A.N. Kholod, V.E. Borisenko, A. Zaslavsky, and F.A. d'Avitaya, Phys. Rev. B **60**, 15 975 (1999).

[29] T. Ouisse, V. Ioannou-Sougleridis, D. Kouvatsos, and A.G. Nassiopoulou, J. Phys. D **33**, 2691 (2000).

[30] C.B. Duke, *Tunneling in Solids; Solid Physics Supplement 10* (Academic Press, New York, 1969).

[31] M. Lininger, A.N. Kholod, S. Menard, V.E. Borisenko, F. Bassani, G. Guirleo, and F.A. d'Avitaya, J. Appl. Phys. **89**, 6281 (2001).

[32] T. Ando, B. Fowler, and F. Stern, Rev. Mod. Phys. **54**, 437 (1982).

[33] G. Bastard, *Wave Mechanics Applied to Semiconductors Heterostructures* (Les Editions de Physique, Paris, 1990).

[34] D.J. BenDaniel and C.B. Duke, Phys. Rev. **152**, 683 (1966).

[35] R.F. Pierret and G.W. Neudeck, *Modular Series On Solid State Devices* (Addison-Wesley, London, 1989).

[36] N.W. Aschroft and N.D. Mermin, *Solid State Physics* (Holt-Saunders, Tokyo, 1981).

[37] V. Mitin, V. Kochelap, and M. Stroscio, *Quantum Heterostructures* (Cambridge University Press, Cambridge, 1999).

[38] E. Molinari and A. Fasolino, in *Spectroscopy of Semiconductor Microstructures*, edited by G. Fasol, A. Fasolino, and P. Lugli (Plenum Press, New York, 1989).

[39] M.V. Fischetti and D.J.D. Maria, Solid-State Electron **31**, 629 (1988).

[40] L. Reggiani, *Hot-Electron Transport in Semiconductors* (Springer, Berlin, 1985).

[41] A. Dargys and J. Kundrotas, *Handbook of Physical Properties of Ge, Si, GaAs* (Science and Encyclopedia Publishers, Vilnius, 1994).

[42] M. Hirose, Mater. Sci. Eng., B **B41**, 35 (1996).

[43] B. Brar, G.D. Wilk, and A.C. Seabaugh, Appl. Phys. Lett. **69**, 2728 (1996).

[44] J.B. Xia and K.W. Cheah, Phys. Rev. B **56**, 14 925 (1997).

[45] C. Jacoboni and L. Reggiani, Rev. Mod. Phys. **55**, 645 (1983).

[46] H.T. Grahn, K. von Klitzing, K. Ploog, and G.H. Döhler, Phys. Rev. B **43**, 12 094 (1991).

[47] S. Rott, P. Binder, N. Linder, and G.H. Döhler, Physica E (Amsterdam) **2**, 511 (1998).

[48] L. Esaki and R. Tsu, IBM J. Res. Dev. **14**, 61 (1970).

[49] A. Wacker, A.-P. Jahuo, S. Rott, A. Markus, P. Binder, and G.H. Dohler, Phys. Rev. Lett. **83**, 836 (1999).

[50] F. Reif, *Fundamentals of Statistical and Thermal Physics* (McGraw-Hill, New York, 1965).

[51] C. Jacoboni, R. Brunetti, P. Bordone, and A. Bertoni, in *Topics in High Field Transport in Semiconductors*, edited by K. Brennan and P.P. Ruden (World Scientific, Singapore, 2001).

[52] P. Bordone, A. Bertoni, R. Brunetti, and C. Jacoboni, VLSI Design **13**, 211 (2001).

[53] The assumption of localization of electron, inside a given layer, may cause problems with the uncertainty relation that would require very large momentum values. However, the analysis of quantum transport in terms of the Wigner Function (Refs. 51,52)

shows that even single electrons can be correctly described in terms of a ''cloud'' of charge, or, equivalently, in terms of a quantum distribution whose single points behave very much like virtual classical particles; they are accelerated, by smooth potential, as classical particles and are scattered by fast varying potentials or phonons with a mechanism very similar to that described in semiclassical particles. The difficulty remains that during the duration of the electron-phonon interaction, the virtual particles may move from a layer to a different one. This consideration may suggest that a quantum treatment of transport in superlattices may be desirable. On the other hand, the assumption of phonon scattering localized in a single layer may also be justified by the consideration that owing to the flat dispersion of the optical-phonon modes, these lattice vibrations can be reasonably well described by the Einstein model of localized harmonic oscillators.